

ARTICLE



# Transplantation of olfactory mucosa mesenchymal stromal cells repairs spinal cord injury by inducing microglial polarization

Xin Wang<sup>1,2,3</sup>, Chun-Gu Hong<sup>3</sup>, Ran Duan<sup>1,3</sup>, Zhi-Lin Pang<sup>1,3</sup>, Min-Na Zhang<sup>1,3</sup>, Hui Xie<sup>1,2,3,4,6</sup>✉ and Zheng-Zhao Liu<sup>5,6</sup>✉

© The Author(s), under exclusive licence to International Spinal Cord Society 2024

## STUDY DESIGN: Animal studies

**OBJECTIVES:** To evaluate the therapeutic effect of olfactory mucosa mesenchymal stem cell (OM-MSCs) transplantation in mice with spinal cord injury (SCI) and to explore the mechanism by which OM-MSCs inhibit neuroinflammation and improve SCI.

**SETTING:** Xiangya Hospital, Central South University; Affiliated Hospital of Guangdong Medical University.

**METHODS:** Mice (C57BL/6, female, 6-week-old) were randomly divided into sham, SCI, and SCI + OM-MSC groups. The SCI mouse model was generated using Allen's method. OM-MSCs were immediately delivered to the lateral ventricle after SCI using stereotaxic brain injections. One day prior to injury and on days 1, 5, 7, 14, 21, and 28 post-injury, the Basso Mouse Scale and Rivlin inclined plate tests were performed. Inflammation and microglial polarization were evaluated using histological staining, immunofluorescence, and qRT-PCR.

**RESULTS:** OM-MSCs originating from the neuroectoderm have great potential in the management of SCI owing to their immunomodulatory effects. OM-MSCs administration improved motor function, alleviated inflammation, promoted the transformation of the M1 phenotype of microglia into the M2 phenotype, facilitated axonal regeneration, and relieved spinal cord injury in SCI mice.

**CONCLUSIONS:** OM-MSCs reduced the level of inflammation in the spinal cord tissue, protected neurons, and repaired spinal cord injury by regulating the M1/M2 polarization of microglia.

*Spinal Cord* (2024) 62:429–439; <https://doi.org/10.1038/s41393-024-01004-6>

## INTRODUCTION

Spinal cord injury (SCI) leads to permanent and severe autonomic, sensory, and motor dysfunction owing to the inability of the adult mammalian central nervous system (CNS) to regenerate lost neurons or reconstruct neural circuits [1]. Inflammation causes secondary tissue damage to injured spinal cords. Reducing inflammation can enhance neuroprotection, promote axonal regeneration, and facilitate functional recovery after SCI [2]. Microglia are resident macrophages in the spinal cord and brain, and serve as the primary immune defense in the CNS [3]. There are two types of microglia: M1 proinflammatory microglia and M2 anti-inflammatory microglia. Microglia can exert both neurotoxic and neuroprotective effects, depending on their polarization [4]. Activated M1 microglia release proinflammatory mediators such as interleukin 6 (IL6), interleukin 1B (IL1B), and tumor necrosis factor (TNF). In contrast, M2 microglia release anti-inflammatory mediators, including interleukin 10 (IL10) and interleukin 4 (IL4) [5]. Therefore, transformation of the microglia into the M2 phenotype is an effective therapeutic approach for SCI.

Mesenchymal stromal cells (MSCs) exert immunomodulatory functions that extend to wound healing and contribute to reducing scar formation [6]. Transplantation of bone marrow mesenchymal stromal cells (BMSCs) or administration of paracrine factors isolated from BMSCs, such as epidermal growth factor, ciliary-derived neurotrophic factor, fibroblast growth factor 2, insulin-like growth factor 1, and osteopontin, can restore a healthy microenvironment and promote wound healing in injured tissues [7–9]. In addition, MSC transplantation benefits SCI by inhibiting inflammation, restoring the local blood supply, and facilitating axonal regeneration throughout the entire SCI [10, 11].

Olfactory mucosa MSCs (OM-MSCs) are olfactory ectomesenchymal stromal cells (OE-MSCs) that reside in the lamina propria of the olfactory mucosa [12, 13]. OM-MSCs offer several advantages, including their origin from the neuroectoderm, easy accessibility under local anesthesia, through noninvasive endoscopic procurement, continuous proliferation throughout life, the exhibition of osteogenic and neurogenic properties, and easy amplification in vitro for autologous transplantation [12, 14]. OM-MSCs augment

<sup>1</sup>Department of Sports Medicine, Xiangya Hospital, Central South University, Changsha, Hunan 410008, China. <sup>2</sup>Department of Orthopedics, Xiangya Hospital, Central South University, Changsha, Hunan 410008, China. <sup>3</sup>Movement System Injury and Repair Research Center, Xiangya Hospital, Central South University, Changsha, Hunan 410008, China. <sup>4</sup>National Clinical Research Center for Geriatric Disorders, Xiangya Hospital, Central South University, Changsha, Hunan 410008, China. <sup>5</sup>Guangdong Provincial Key Laboratory of Autophagy and Major Chronic Non-Communicable Diseases, Key Laboratory of Prevention and Management of Chronic Kidney Disease of Zhanjiang City, Institute of Nephrology, Affiliated Hospital of Guangdong Medical University, Zhanjiang, Guangdong 524001, China. <sup>6</sup>These authors contributed equally: Hui Xie, Zheng-Zhao Liu. ✉email: [huixie@csu.edu.cn](mailto:huixie@csu.edu.cn); [liuzhengzhao@gdmu.edu.cn](mailto:liuzhengzhao@gdmu.edu.cn)

Received: 11 January 2024 Revised: 27 May 2024 Accepted: 3 June 2024  
Published online: 7 June 2024

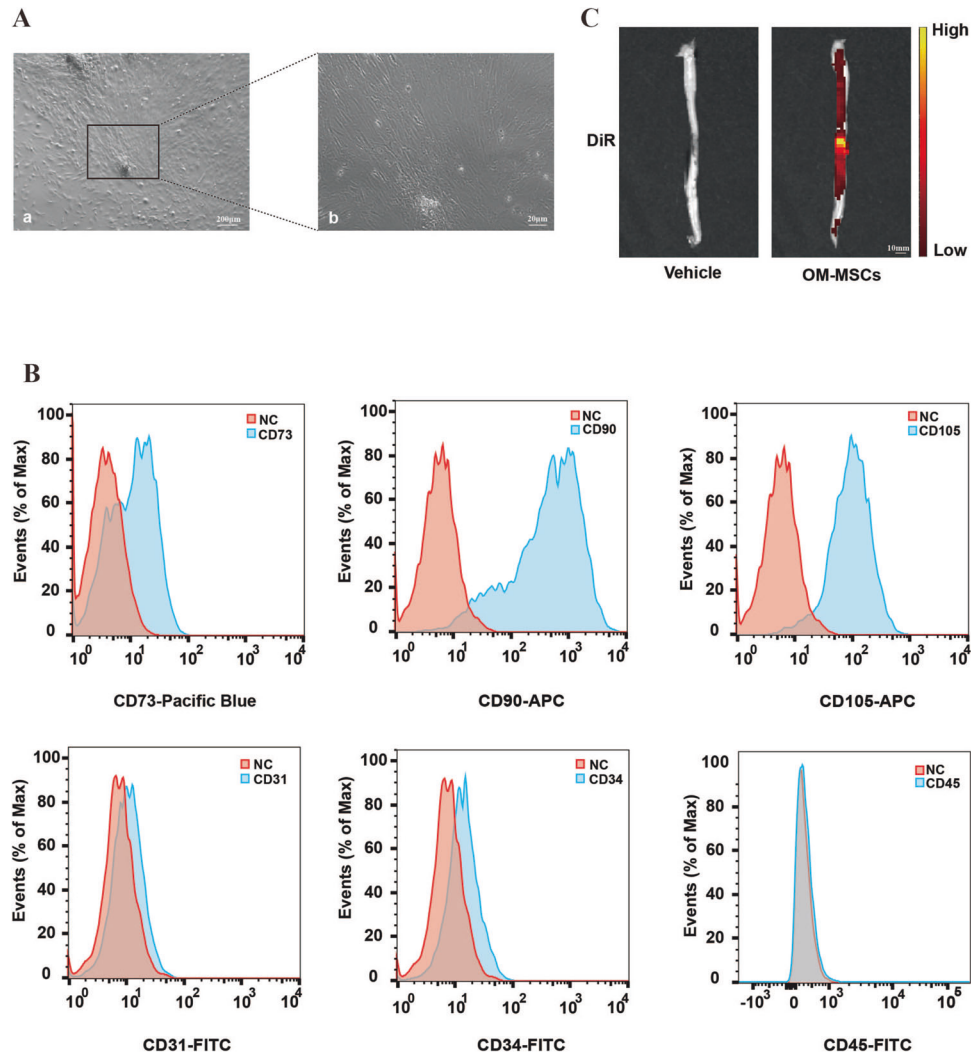


**Fig. 1 Identification and tracking of OM-MSCs delivered to the spinal cord injury site.** **A** Representative images showing the spindle-like morphology of OM-MSCs. Scale bar: 200  $\mu\text{m}$  (A, a), 20  $\mu\text{m}$  (A, b). **B** Flow cytometry analysis of the cell surface markers of OM-MSCs ( $\text{CD73}^+$ ,  $\text{CD90}^+$ ,  $\text{CD105}^+$ ,  $\text{CD31}^-$ ,  $\text{CD45}^-$ , and  $\text{CD34}^-$ ). The isotype controls are represented as solid red curve and the test samples are represented as solid blue curves. **C** Representative ex vivo fluorescent images of the spinal cord from mice treated with vehicle or DiR-labeled OM-MSCs by brain stereotaxic injection. Scale bar: 10 mm.

neurogenesis and neural network recovery [15]. Several studies have demonstrated the beneficial effects of OM-MSCs in the treatment of nervous system diseases [16–20]. Lindsay et al. reported that OM-MSCs have a high expression level of CXCL12, which induces microglia to polarize towards a more anti-inflammatory phenotype [18]. Our data indicate that OM-MSC transplantation restrains neuroinflammation following SCI by promoting the transformation of microglia from the M1 to the M2 phenotype, thereby relieving SCI. Therefore, OM-MSCs may have remedial potential for SCI.

## METHODS

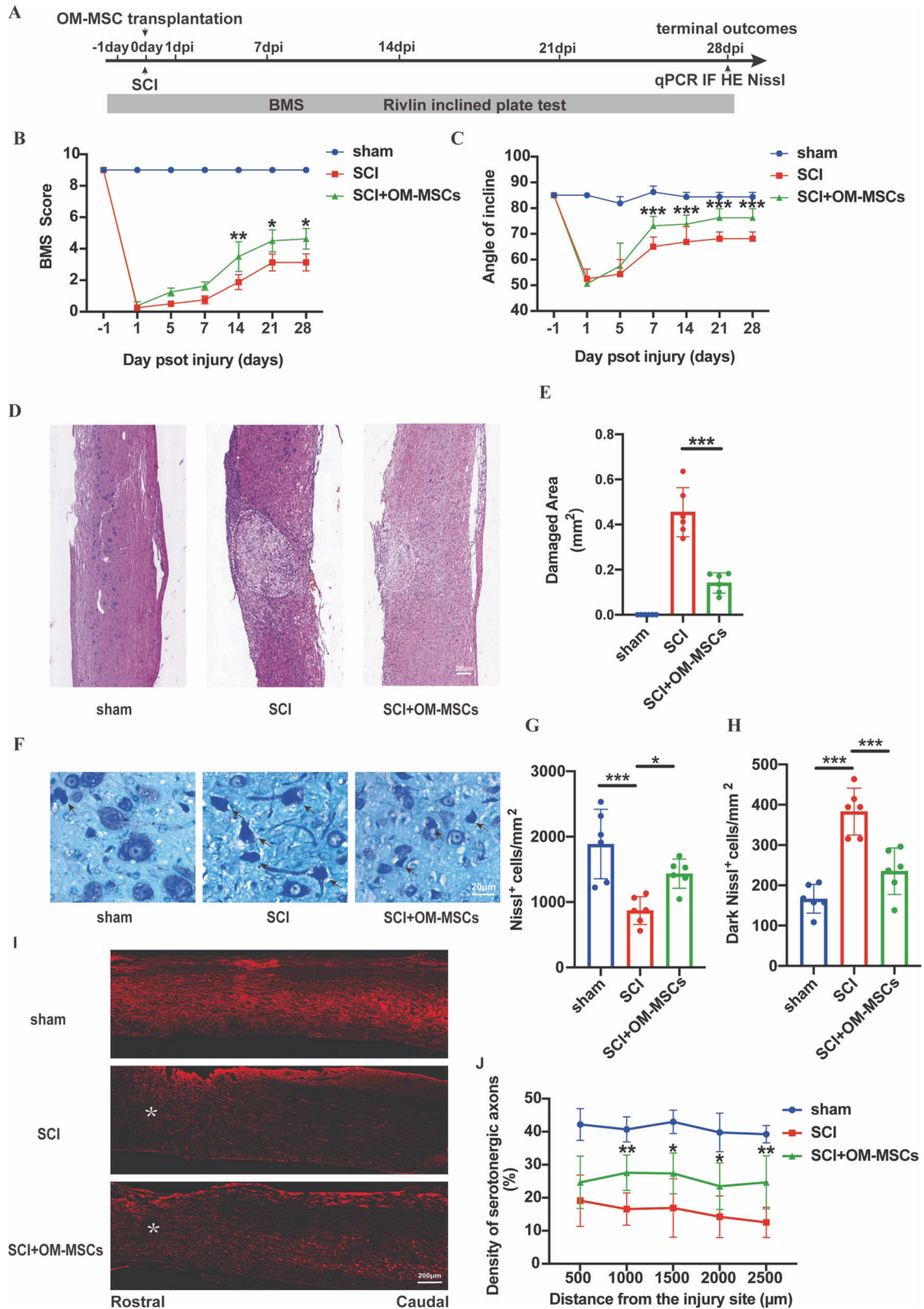
### Preparation of the mouse SCI model and allocation of experimental groups

The SCI mouse model was generated using Allen's method as previously described [21]. Mice (C57BL/6, female, 6-week-old, 18–25 g) were obtained from Hunan SJA Laboratory Animal Co., Ltd. (Hunan, China). The mice were housed in cages maintained at 22°C with 50% humidity and were subjected to a light-dark cycle for 12/12 h each day. Briefly, an Allen's percussion device (percussion stick: weight of 10 g, diameter of 3.9 mm; gasket: height of 4 mm, diameter of 1.8 mm) was used to strike the

T10 spinal cord vertically at a height of 1 cm. Following successful modeling the mouse exhibited spasmodic tail swinging, convulsions in its lower limbs, and the appearance of a hematoma at the injury site. The bladders of the mice were manually voided thrice a day until reflexive bladder control was achieved. The animals were randomly divided into three groups: sham (treated with PBS), SCI (the SCI model treated with PBS), and SCI + OM-MSCs (the SCI model treated with OM-MSCs). The investigator was blinded to the group allocation during the experiment and when assessing the outcome. All animal experiments were approved by the Ethical Review Board of Xiangya Hospital of Central South University (No. 2017121175).

### Brain stereotaxic injection

OM-MSCs were immediately delivered to the lateral ventricle after SCI using brain stereotaxic injection as previously described [22]. Briefly, mice were fixed in a stereotaxic instrument (Yuyan Instruments Co., Ltd., Shanghai, China) after being anesthetized with 0.3% pentobarbital sodium (20  $\mu\text{L/g}$ ). We performed the craniotomy after the midline incision, located the lateral ventricle at 1.5 mm beside the sagittal suture, 2.0 mm below the bregma, and 2.5 mm in depth. Using a hand-held cranial drill and a 0.5 mm drill bit, a hole was drilled. OM-MSCs (2  $\mu\text{L}$ ,  $1 \times 10^5$  cells/ $\mu\text{L}$ ) were injected into the lateral ventricle at a rate of 1.0  $\mu\text{L}$  every 3 min. Finally, the wound was sutured and decontaminated with iodophor.



**OM-MSc isolation and identification**

OM-MSCs were isolated from mice, as previously described [23]. Briefly, the mouse was anesthetized with 20 µL/g 0.3% pentobarbital sodium, and the bone covering the nasal cavity was subsequently removed to expose the nasal septum. The olfactory mucosa (the region within the ceiling of the oral cavity, cribriform plate, arc of the perpendicular plate, and respiratory

mucosa) was isolated and soaked in Dulbecco's Modified Eagle Medium/ Nutrient Mixture F-12 (DMEM/F12, Pricella, PM150310) containing 2% fetal bovine serum (FBS; CellMax, SA211.02). After rinsing twice with culture medium to remove mucus, the olfactory epithelium (gray) was removed from the underlying lamina propria (brown) under a dissecting microscope. Subsequently, the lamina propria was chopped and incubated with

**Fig. 2 OM-MSCs promote neural rehabilitation and functional behavioral recovery post SCI.** **A** Timeline of the experimental protocol. **B, C** BMS and the Rivlin inclined plate test were used to functionally grade the mice on day 1 prior SCI and days 1, 5, 7, 14, 21, and 28 post SCI in the sham, SCI, and SCI + OM-MSCs groups.  $n = 6$  per group. **D** Representative images showing HE staining post SCI. Scale bar: 200  $\mu\text{m}$ . **E** Quantification of the damaged area on day 28 post SCI,  $n = 6$  per group. **F** Representative images showing Nissl staining after SCI. Scale bar: 20  $\mu\text{m}$ . **G** Quantification of the Nissl<sup>+</sup> cells in different groups post SCI.  $n = 6$  per group. **H** Quantification of the dark Nissl<sup>+</sup> cells in different groups post SCI.  $n = 6$  per group. **I** Representative images showing serotonergic axons on day 28 post staining with anti-serotonin (anti-5-HT) antibody. White stars indicate the lesion site, serotonergic axons are represented in red. Scale bar: 200  $\mu\text{m}$ . **J** Quantitative analysis of the density of serotonergic axons in the spinal cord on day 28 post SCI (quantify the 5-HT-positive area within the segmented area, the spinal cord was divided into 5 segments from the injury site to the caudal ends),  $n = 6$  per group. All data are presented as mean  $\pm$  sd. \*  $P < 0.05$ , \*\*  $P < 0.01$ , \*\*\*  $P < 0.001$ .

type II collagenase (Gibco, 17101015, 1 mg/mL) in 4 mL DMEM/F12 containing 2% FBS at 37 °C for 1 h. To terminate the dissociation, 9 mL of calcium- and magnetic-free PBS was added and centrifuged at 200  $\times$   $g$  for 5 min. The cells were resuspended in DMEM/F12 culture medium supplemented with 10% FBS, 100  $\mu\text{g}/\text{mL}$  streptomycin, and 100 U/mL penicillin (Solarbio Life Science, P1400) and plated on a plastic culture flask. After 2 weeks, the adherent cells were collected using 0.25% trypsin-EDTA (Gibco, 12604021) and passaged at a split ratio of 1:3. Fluorescence-activated cell sorting (FACS) was used to analyze cells harvested by trypsinization at passage 4. Samples ( $1 \times 10^6$  cells) were stained with FITC-conjugated anti-CD31 (R&D, FAB3628G), anti-CD45 (BD, 561088; 1:200), anti-CD34 FITC-conjugated (BD, 560238; 1:100), anti-CD73 FITC-conjugated (BD, 550741; 1:200), anti-CD105 APC-conjugated (BD, 562761; 1:200), and anti-CD90 (Biolegend, 105305). The cells were examined using a flow cytometry system (BD, FACS Canto II), and the data were analyzed using FlowJo software (BD, Version 10.5.3). Isolated OM-MSCs were characterized as CD73<sup>+</sup>, CD90<sup>+</sup>, CD105<sup>+</sup>, CD31<sup>-</sup>, CD45<sup>-</sup>, and CD34<sup>-</sup>. The cell gating method was based on comparison with isotype controls.

### OM-MSCs tracing

OM-MSCs (2  $\mu\text{L}$ ,  $1 \times 10^5$  cells/ $\mu\text{L}$ ) were labeled with lipophilic dye 1,1-dioctadecyl-3,3,3-tetramethylindotricarbocyanine (DiI, 5.0  $\mu\text{g}/\text{mL}$ , Santa Cruz) in 1 mL PBS at 37 °C for 30 min. OM-MSCs were washed twice (1200 rpm, 3 min, 25 °C) with PBS to remove excess dye and then administered via brain stereotaxic injection. Equal amounts of solvent were used to treat the control mice. The spinal cord was collected after 24 h transplantation, and fluorescent signals in the spinal cord were detected using a fluorescence tomography imaging system (FMT-4000; PerkinElmer, USA).

### Tissue procurement

One month after receiving OM-MSC transplantation, the mice were deeply anesthetized with 0.3% pentobarbital sodium (20  $\mu\text{L}/\text{g}$ ) and euthanized. The mice were transcardially perfused with 0.9% saline and 4% paraformaldehyde, and the spinal cord surrounding the injury site was dissected and post-fixed in 4% paraformaldehyde for 4–6 h.

### H&E staining and Nissl staining

Tissue samples were embedded in paraffin and cut into 5.0  $\mu\text{m}$  thick sections. After being heated for 1 h at 60 °C, the paraffin sections were deparaffinized with xylene for 30 min, followed by rehydration in a graded series of alcohols (100%, 100%, 95%, 95%, 80%, 70%, and 50%) for 5 min each. Double-distilled water was used to rinse sections twice. For hematoxylin and eosin (H&E) staining, samples were stained with hematoxylin for 1 min and eosin (Sigma–Aldrich) for 2 min. For Nissl staining, the Nissl substance in the sections was stained with methylene blue (Solarbio, G1434) for 1 min. The sections were then rinsed twice with distilled water and sealed with neutral balsam. An inverted microscope (Leica DMI4000B) was used to capture images of both H&E- and Nissl-stained sections. The lesion areas and neuron numbers were quantified using Image-Pro Plus 6.0 (Media Cybernetics, Rockville, MD, USA). Six mice were used per group.

### Immunofluorescence

Tissue samples were dehydrated in 30% sucrose solutions and rapidly frozen after embedding with an optimal cutting temperature compound. Subsequently, they were cut into 10.0  $\mu\text{m}$  sections and incubated overnight at 4 °C with an IBA1 antibody (Abcam, ab178847), washed, and treated with secondary antibodies at 37 °C for 1 h. Nuclei were stained with DAPI (VectorLabs, H-1200). An ApoTome.2 imaging system (Zeiss,

Germany) was used to capture the fluorescence images. Immunofluorescence assays for 5-HT (ImmunoStar, 20080), ARG1 (Santa Cruz Biotechnology, sc-271430), and NOS2 (Abcam, ab178945) in the spinal cord were performed as described above.

### qRT-PCR

The standard TRIzol method was used for total RNA extraction from mouse spinal cords or cells, as previously described [22]. Expression levels were normalized to the internal control (*Gapdh*). Amplification (40 cycles of 15 s at 95 °C and 60 s at 60 °C) was followed by denaturation (2 min at 95 °C). The primers were synthesized by Sangon Biotech (Shanghai, China). The primer sequences are listed in Supplementary Table 1.

### Cell coculture

To study cell-cell interactions, cell co-culture was performed using a Transwell assay as previously described [24]. BV-2 cells were seeded in a lower well ( $10^6$  cells/well) and treated with 200 ng/mL lipopolysaccharide (LPS) for 24 h to induce BV-2 polarization. The cells were then co-cultured with OM-MSCs in the upper wells ( $10^5$  cells/well) for 24 h.

### Hindlimb exercise score

Basso Mouse Scale (BMS) was used to determine hindlimb locomotion function [25]. The mice were placed on a circular platform with a diameter of 2 m. The scores ranged from 0 (complete paraplegia) to 9 (normal function). Each group was scored 1 day prior to injury and on days 1, 5, 7, 14, 21, and 28 post-injury (dpi). The hind limb exercise score was evaluated by two trained observers who were blinded to the experimental conditions.

### Rivlin inclined plate test

The mice were positioned on a wooden plate with a rubber covering, and an inclined plate was rotated at its base. The body axis was aligned parallel to the vertical axis of the plate. In each trial, the plate angle was increased by 5°. The functional score was determined based on the maximum position that the mouse maintained for >5 s. The mean value for each mouse was calculated from three measurements. Each group was scored 1 d prior to injury and on days 1, 5, 7, 14, 21, and 28 dpi.

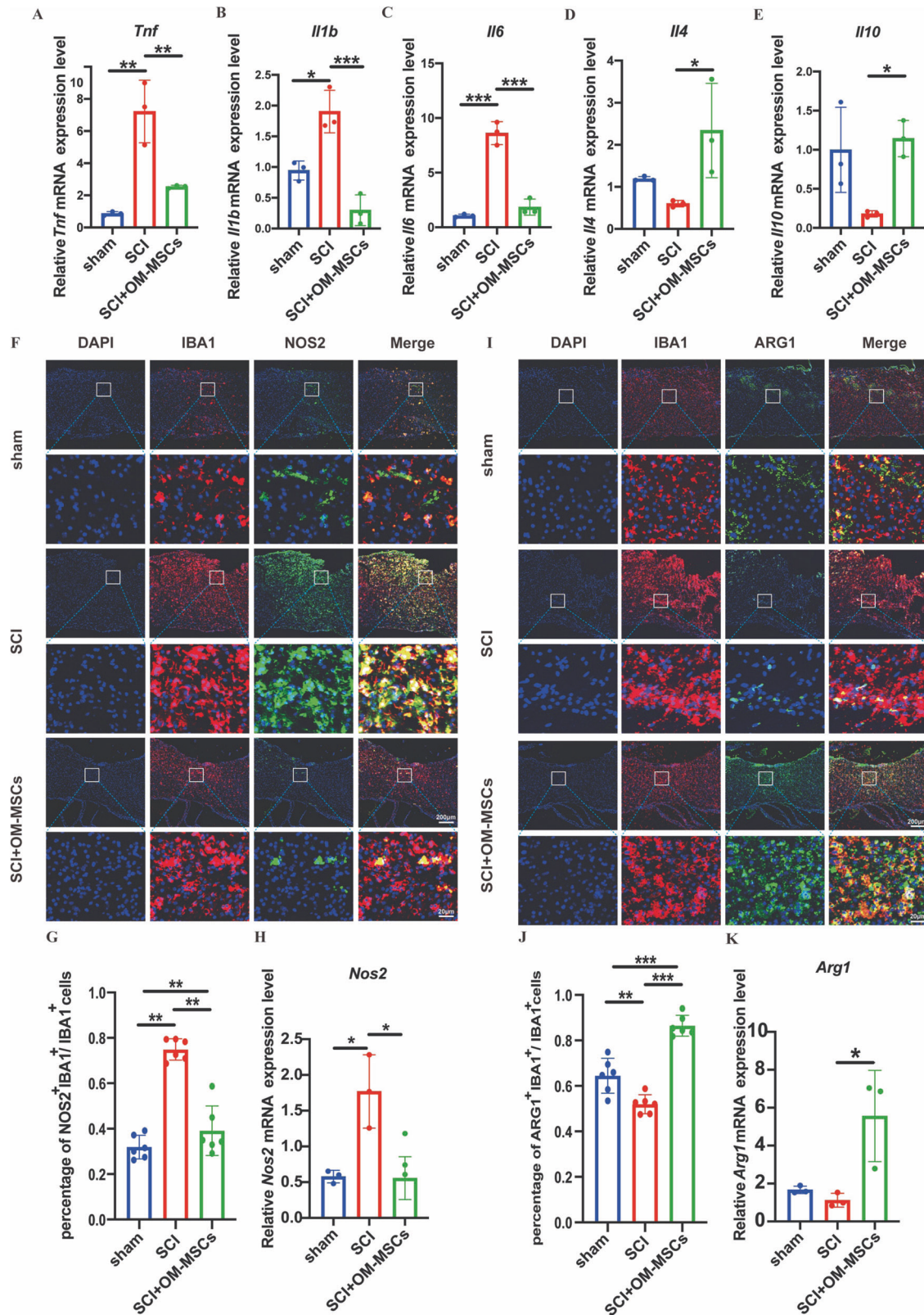
### Statistical analysis

Data were analyzed using Prism 8 (GraphPad Software) and presented as mean  $\pm$  standard deviation. An unpaired t-test was used to compare the two groups. Significance was determined using analysis of variance (ANOVA) while performing multiple comparisons. One-way ANOVA (one variance) or two-way ANOVA (more than one variance) with Holm–Sidak post hoc analysis was used to determine statistical significance. In all experiments, statistical significance was determined as \* $P < 0.05$ , \*\*  $P < 0.01$ , \*\*\* $P < 0.001$ , and ns = not significant.

## RESULTS

### Identification of OM-MSCs

OM-MSCs were isolated from the nasal mucosa of mice. To confirm the identity of the isolated cells as OM-MSCs, the expression of various OM-MSC markers (CD73<sup>+</sup>, CD90<sup>+</sup>, CD105<sup>+</sup>, CD31<sup>-</sup>, CD45<sup>-</sup>, and CD34<sup>-</sup>) was analyzed using FACS [20]. OM-MSCs exhibit high proliferative ability [26, 27]. Our results revealed that OM-MSCs were sparingly attached to culture dishes and displayed a characteristic spindle-like morphology (Fig. 1A). The isolated OM-MSCs were positive for CD73, CD90, and CD105, and



negative for CD31, CD34, and CD45 (Fig. 1B) based on flow cytometry analysis, suggesting that the isolated primary OM-MSCs exhibit typical MSC characteristics. The OM-MSCs were then labeled with DiI dye to examine their migration to the spinal cord tissues after delivery to the lateral ventricle using brain stereotaxic

injection. After 24 h of OM-MSC transplantation, strong fluorescent signals indicative of OM-MSCs were detected in the spinal cord tissues upon ex vivo fluorescence imaging (Fig. 1C), suggesting that the cerebrospinal fluid circulates OM-MSCs into the spinal cord.

**Fig. 3 Administration of OM-MSCs following SCI ameliorates inflammation and increases the M2 microglia proportion in vivo.** **A–E** The relative expression level of proinflammatory cytokines and anti-inflammatory cytokines in the sham, SCI, and SCI + OM-MSCs groups on day 28 post SCI,  $n = 3$  per group. **F** Representative coimmunofluorescent staining images of IBA1 (red) and NOS2 (green) in the injured spinal cord lesion areas and the analysis of NOS2-positive microglia in the traumatic lesion area. Low-magnification images are presented with insets at higher magnification in the bottom panels. Nuclei stained with DAPI were shown in blue. Scale bar: 200  $\mu\text{m}$  and 20  $\mu\text{m}$ . **G** Quantification of the percentage of NOS2<sup>+</sup> IBA1<sup>+</sup>/IBA1<sup>+</sup> cells on day 28 post SCI,  $n = 6$  per group. **H** Determination of the *Nos2* mRNA expression level using qRT-PCR,  $n = 3$  per group. **I** Representative of the coimmunofluorescent staining images of IBA1 (red) and ARG1 (green) in the injured spinal cord lesion areas and the analysis of ARG1-positive microglia in the traumatic lesion area. Low-magnification images are presented with insets at higher magnification in the bottom panels. Nuclei stained with DAPI were shown in blue. Scale bar: 200  $\mu\text{m}$  and 20  $\mu\text{m}$ . **J** Quantification of percentage of ARG1<sup>+</sup> IBA1<sup>+</sup>/IBA1<sup>+</sup> cells on day 28 post SCI,  $n = 6$  per group. **K** Determination of *Arg1* mRNA expression level using qRT-PCR,  $n = 3$  per group. All data are presented as mean  $\pm$  sd. \*  $P < 0.05$ , \*\*  $P < 0.01$ , \*\*\*  $P < 0.001$ .

### Administration of OM-MSCs promoted SCI remission

To determine SCI remission following OM-MSC administration, BMS was applied to determine the severity of SCI, along with conducting the Rivlin inclined plate test to evaluate behavioral recovery. Additionally, H&E staining, Nissl, and serotonergic staining were performed to assess scar formation, neuron viability, and serotonergic axon formation, respectively. The mice were randomly divided into three groups: sham (treated with PBS), SCI (SCI + PBS), and SCI + OM-MSCs. Each group was scored 1 day prior to injury and on days 1, 5, 7, 14, 21, and 28 post-injury (dpi) (Fig. 2A). Regarding locomotor recovery, the SCI + OM-MSCs group exhibited higher BMS scores than the SCI group (Fig. 2B). After recording the BMS score, the Rivlin inclined plate test was performed to evaluate nerve healing and its effects on motor function [28]. Mice in the SCI + OM-MSCs group exhibited their capability to maintain their position at a larger angle on an inclined plane than those in the SCI group (Fig. 2C), suggesting the recovery of functional behavior in SCI mice treated with OM-MSCs. For morphological analysis, H&E staining revealed a remarkable shrinkage and reduction of the scar size after OM-MSC administration in SCI mice (Fig. 2D and E). Nissl staining revealed an increase in Nissl<sup>+</sup> cells and a decrease in dark Nissl<sup>+</sup> cells (shrinking neurons with deep staining) in the SCI + OM-MSCs group compared with the SCI group, suggesting significant morphological changes and inhibition of neuronal cell loss at the injury site following OM-MSC treatment in the SCI model (Fig. 2F–H). Furthermore, serotonergic axons were assessed on day 28 post-injury using anti-5-HT antibody staining. In the SCI + OM-MSCs group, serotonergic axons established denser projections than in the SCI group (Fig. 2I, J), suggesting enhanced neural circuit reconstitution after OM-MSC treatment. Overall, our results suggest that OM-MSC administration reduces the severity of SCI by inhibiting neuronal cell loss and promoting axonal regeneration.

### Administration of OM-MSCs reduced the inflammatory response and promoted microglial polarization

To investigate whether OM-MSCs exert their functions by modulating the immune response, we examined inflammatory responses and microglial polarization. The gene expression of anti-inflammatory cytokines (*Il10* and *Il4*) and proinflammatory cytokines (*Il1b*, *Il6*, and *Tnf*) in the spinal cord tissue was measured using qRT-PCR. The mice in the SCI group had higher gene expression levels of proinflammatory cytokines and reduced gene expression levels of anti-inflammatory cytokines than those in the sham group. However, OM-MSC treatment increased anti-inflammatory cytokine gene expression and inhibited proinflammatory cytokine gene expression in SCI mice (Fig. 3A–E). Moreover, MSCs modulate immune function and increase the number of microglial M2 cells [29]. We examined microglial polarization by analyzing M1-associated nitric oxide synthase 2 (*Nos2*) and M2-associated arginase 1 (*Arg1*) gene expression. *Nos2* expression was significantly increased, while the expression of *Arg1* decreased in the SCI group compared to the sham group. Furthermore, *Nos2* expression levels were lower, whereas *Arg1* expression levels were

higher in the SCI + OM-MSCs group than in the SCI group (Fig. 3H and K). Co-immunofluorescence of NOS2 and induction of brown adipocyte 1 (IBA1, a marker of microglia) revealed a decreased M1 proportion in the SCI + OM-MSCs group compared to the SCI group, as indicated by the decreased percentage of IBA1<sup>+</sup> NOS2<sup>+</sup>/IBA1<sup>+</sup> cells (Fig. 3F, G). Co-immunofluorescence analysis of ARG1 and IBA1 demonstrated that the SCI + OM-MSCs group had a higher IBA1<sup>+</sup> ARG1<sup>+</sup>/IBA1<sup>+</sup> cell percentage compared to that in the SCI group (Fig. 3I, J). These results demonstrated that OM-MSC administration inhibited inflammation, decreased the proportion of M1 microglia, and increased the M2 proportion of microglia in the SCI mouse model.

### Administration of OM-MSCs potentiated M2 transformation in BV-2 cells

Next, microglial cells (BV-2) and OM-MSCs were co-cultured in a Transwell plate to determine whether OM-MSCs potentiated the transformation of BV-2 cells into the microglial M2. LPS was added to the cell culture system of BV-2 cells for 24 h to simulate the inflammatory microenvironment following SCI. The inflammatory status was mitigated after co-culture with OM-MSCs, as indicated by the upregulation of anti-inflammation-associated genes (*Il10*, *Il4*) and the downregulation of proinflammation-associated genes (*Il1b*, *Il6*, and *Tnf*) as determined by quantitative RT-PCR (Fig. 4A–E). Furthermore, OM-MSC treatment significantly increased the percentage of M2 microglia and decreased the proportion of M1 microglia, as indicated by the increased ARG1<sup>+</sup> IBA1<sup>+</sup>/IBA1<sup>+</sup> cell percentage and the reduced proportion of NOS2<sup>+</sup> IBA1<sup>+</sup>/IBA1<sup>+</sup> cells (Fig. 4F, G, I and J). Co-culturing with OM-MSCs decreased the expression of *Nos2* and increased the expression of *Arg1* (Fig. 4H, K). In addition to the in vivo finding that OM-MSCs increased M2 proportions and decreased M1 proportions at spinal cord injury sites in SCI mice, our results indicated that OM-MSCs promoted the BV-2's M2 phenotypic transition, resulting in a higher ratio of M2 cells.

### DISCUSSION

SCI is a neurological disorder characterized by high mortality and disability rates. Treatment and rehabilitation are challenging in the treatment of SCI. Our study revealed that OM-MSC administration benefits motor function recovery and promotes nerve repair by inhibiting inflammation and increasing the proportion of M2 microglia in an SCI mouse model.

Epidural electrical stimulation (EES) combined with the sequential reinstatement of neuronal intrinsic growth capacity, growth-supportive substrates, and chemoattraction can promote neuro-rehabilitation in SCI [30, 31]. However, the requirement for a specialized apparatus for EES treatment and the complexity of multiple factor combinations limit its clinical application. Cell transplantation is one of the most explored approaches in current SCI treatment research, and MSC transplantation is the most concerned. MSC can be obtained from various tissues, including bone marrow, adipose tissue, umbilical cord blood, and dental pulp, among others. MSC transplantation benefits SCI treatments

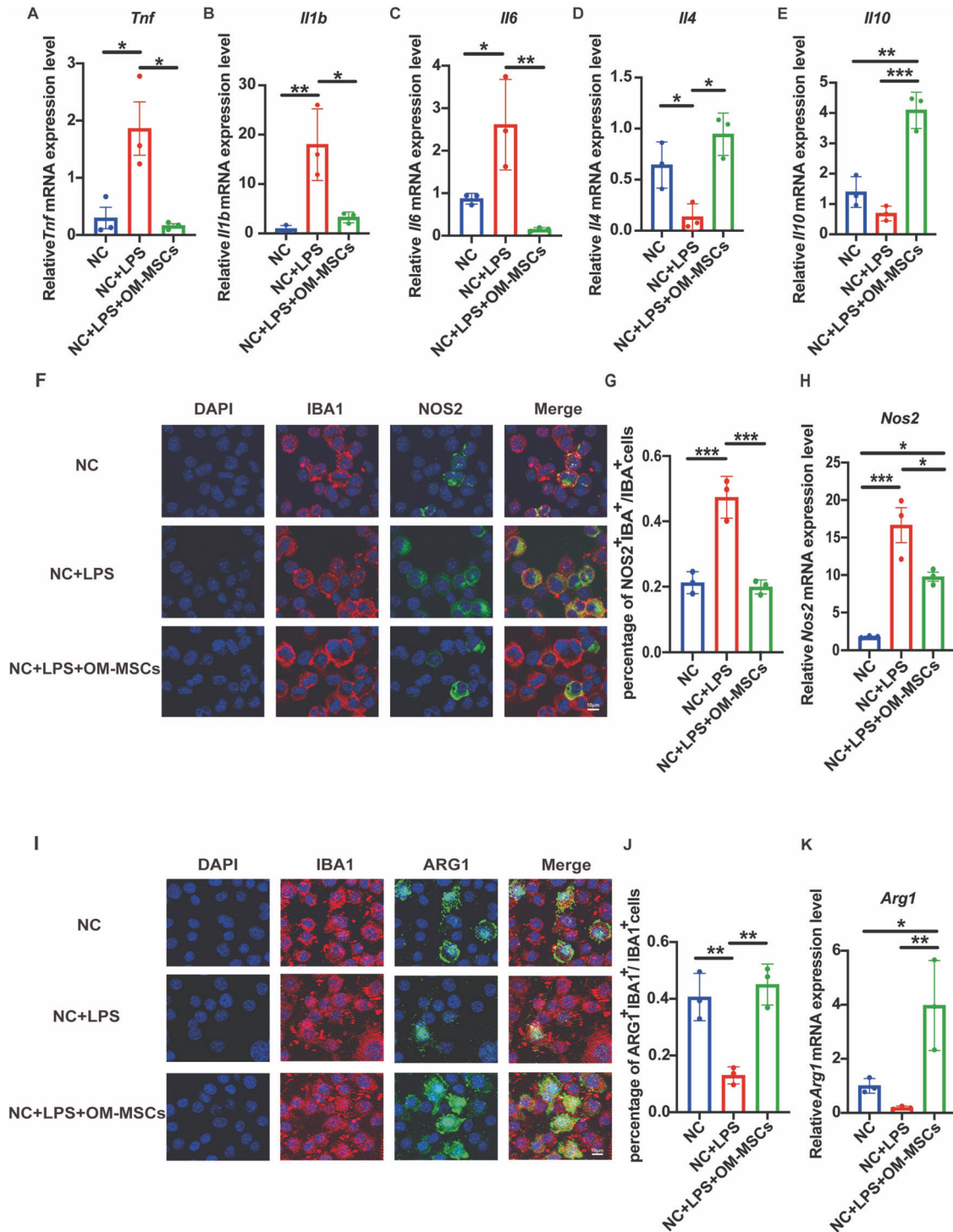


**Fig. 4 Administration of OM-MSCs ameliorates inflammation and promotes the transformation of BV-2 cells from the M1 to M2 phenotype in vitro.** **A–E** The relative expression level of proinflammatory cytokines and anti-inflammatory cytokines in the NC, NC + LPS, and NC + LPS + OM-MSCs groups,  $n = 3$  per group. **F** Representative of the coimmunofluorescent staining of IBA1 (red) and NOS2 (green) in BV-2 cells cocultured with or without OM-MSCs. Nuclei stained with DAPI were shown in blue. Scale bar: 10  $\mu\text{m}$ . **G** Quantification of percentage of NOS2<sup>+</sup> IBA<sup>+</sup>/IBA<sup>+</sup> cells,  $n = 3$  per group. **H** Determination of *Nos2* mRNA expression level using qRT-PCR in the NC, NC + LPS, and NC + LPS + OM-MSCs groups,  $n = 3$  per group. **I** Representative of the coimmunofluorescent staining images of IBA1 (red) and ARG1 (green) in BV-2 cells cocultured with or without OM-MSCs. Nuclei stained with DAPI were shown in blue. Scale bar: 10  $\mu\text{m}$ . **J** Quantification of percentage of ARG1<sup>+</sup> IBA<sup>+</sup>/IBA<sup>+</sup> cells,  $n = 3$  per group. **K** Determination of *Arg1* mRNA expression level using qRT-PCR in the NC, NC + LPS, and NC + LPS + OM-MSCs groups,  $n = 3$  per group. All data are presented as mean  $\pm$  sd. \*  $P < 0.05$ , \*\*  $P < 0.01$ , \*\*\*  $P < 0.001$ .

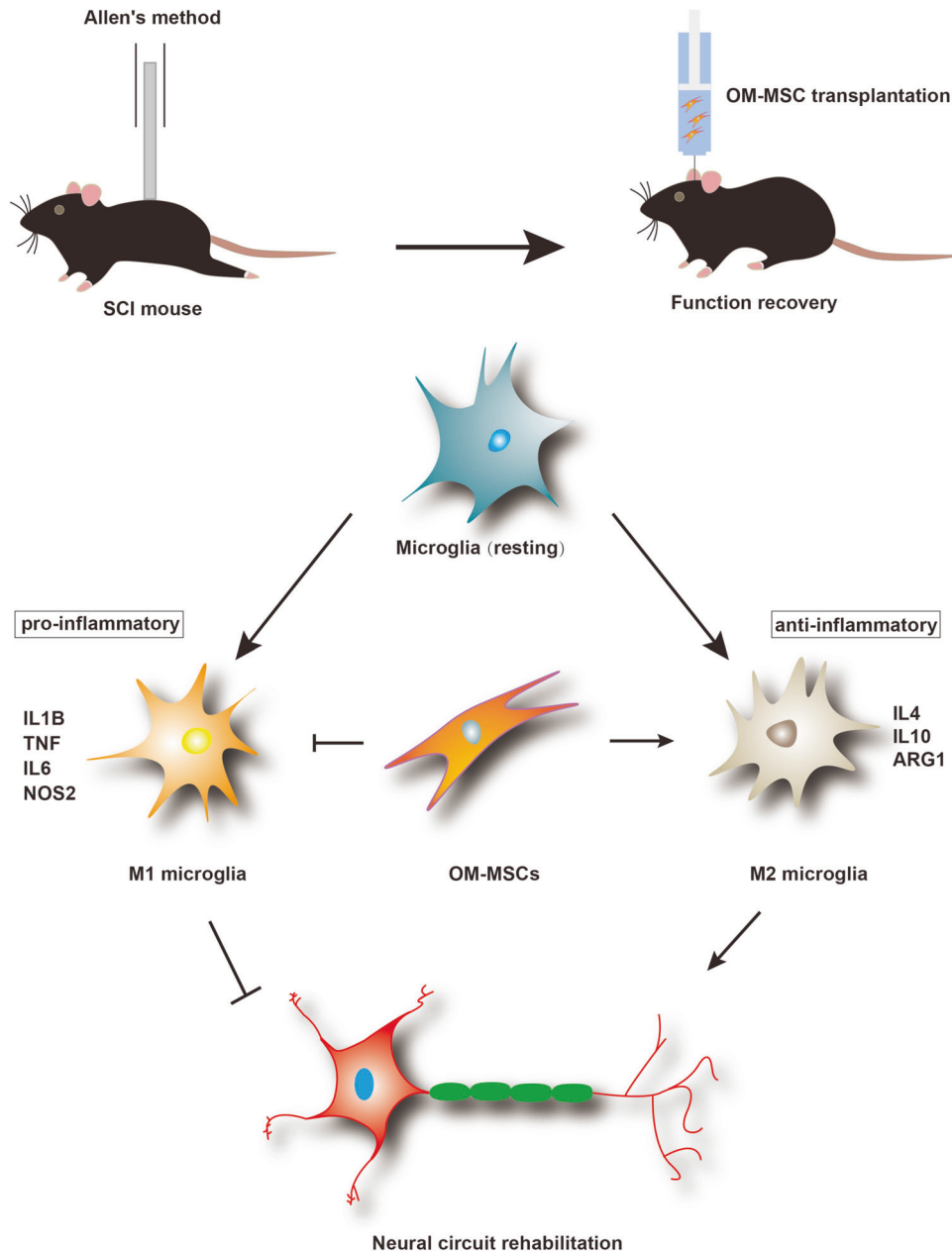


**Fig. 5** OM-MSc treatment improves SCI by inducing microglial polarization, inhibiting inflammation, and rebuilding the neural circuit.

owing to its simple surgical procedures. However, how to overcome clinical safety and efficacy in MSCs therapy for spinal cord injury is a matter that must be carefully considered, such as combinatorial use of rehabilitation, and overcome the potential risks of tumor formation [32]. MSCs from different tissue sources may exhibit variations in their differentiation capacity towards specific cell lineages [33]. For example, MSCs derived from bone marrow are well-known for their ability to differentiate into bone, cartilage, and adipose tissue [34], whereas MSCs from adipose tissue may have a higher propensity for adipogenic differentiation [35]. Similarly, MSCs from umbilical cord blood may show enhanced hematopoietic support capabilities due to their origin [36]. Unlike BMSCs, which originate from the mesoderm, OM-MSCs are an alternative source for the renewal of neurons because they originate from the neural crest. Autologous transplantation of OM-MSCs promotes movement and axogenesis in rats with

neurological injury [37]. Human OM-MSCs have been used in a human model of SCI and have demonstrated potential effects on the recovery of segmental neurological function [38]. Our data demonstrate that OM-MSc administration promotes recovery in SCI mice (Fig. 5).

Stem cells perform their functions via different pathways. Neural progenitor cells differentiate into neuronal and glial cells in the lesion site of the spinal cord [39], while natural stem cells promote macrophage migration depending on the UTX-NF- $\kappa$ B signaling pathway in SCI mice [40]. OM-MSCs stimulate endogenous neurogenesis, restore synaptic transmission [15, 41], and promote myelination and remyelination in the CNS [19]. In addition, OM-MSCs can differentiate into motor neuron-like cells [42]. We found that OM-MSCs impeded inflammation and increased the proportion of M2 microglia (Fig. 5), which is consistent with a previous report showing that MSCs restrain



microglial M1 activation and augment M2 polarization [18, 43–46]. Studies show the beneficial effects of MSC transplantation is through the secretion of protective and trophic factors, which have reparative effects on injured tissues [47]. Exosomes are an important pathway for the secretion of paracrine molecules, and OM-MSC-derived exosomes contain various inflammation-regulating proteins such as Haptoglobin-related protein (HPR), which can modulate the activity of macrophages and suppress inflammation, Alpha-2-macroglobulin ( $\alpha$ 2M) interacts with inflammatory mediators to regulate the intensity and duration of inflammation [48]. These components may be important substances in inducing M1/M2 polarization of microglial cells. Interestingly, the exosomes of OM-MSCs also contain various neurotrophic-related proteins such as Guanine nucleotide-binding protein subunit gamma-12 (GNG12), Sodium-coupled neutral amino acid transporter 2 (SLC38A2), Neprilysin, etc [48]. Therefore, OM-MSCs may also participate in the repair of nerve injury by secreting neurotrophic factors. Our limitation is that we did not examine other possible pathways.

Olfactory ensheathing cells (OECs) are cells of olfactory origin used in SCI [49, 50]. OEC transplantation has emerged as a beneficial approach for SCI therapy because it reduces inflammation [51, 52], and promotes the expression of high levels of growth factors [53]. While procurement of OECs from the olfactory bulb is invasive and impairs olfactory sensation, the purity and proliferative ability of these cells is poor when cultured in vitro [53]. In contrast, obtaining OM-MSCs from the nasal cavity is considered a minimally invasive procedure with a low-risk profile. OM-MSCs are characterized by a high proliferation rate and purity when cultured in vitro. Thus, OM-MSCs from the olfactory mucosa are a more suitable option than OECs for relieving SCI.

The delivery method for OM-MSCs had a significant influence on the outcomes. In our study, we transplanted  $2 \times 10^5$  OM-MSCs into the lateral ventricle via brain stereotaxic injection. We found that OM-MSCs reached the site of spinal cord injury 24 h after transplantation through fluorescence tomography imaging system. MSCs typically possess strong homing ability and can migrate to lesion sites [54]. This homing ability is mediated by chemotactic factors and inflammatory factors [55]. Factors such as vascular endothelial growth factor and hepatocyte growth factor released at the injury site can attract MSCs [55, 56]. The SDF-1 $\alpha$ /CXCR4 axis, substance P, and granulocyte colony-stimulating factor can also influence MSC migration [57–59]. OM-MSCs may possess similar homing capabilities, allowing them to migrate from the lateral ventricle to the site of spinal cord injury. However, the detailed mechanism still needs further investigation. However, we did not perform a comparison with intrathecal injection, which has demonstrated to be effective for OM-MSCs to migrate to lesioned regions of the CNS [60]. Intravenous and intraperitoneal injections are limited by the fact that OM-MSCs cannot penetrate the blood-brain barrier and thus cannot migrate to the spinal injury site. Zhang et al. showed that intravenous administration of OEC reduces neuroinflammation in SCI [51, 61]. This phenomenon may be interpreted as an improvement in the local microenvironment following the circulation of OM-MSCs to the lesion site in the spinal cord.

Furthermore, OM-MSC transplantation combined with the addition of auxiliary conductive hydrogels at the injury site [62], the addition of neural differentiation promoting factors (such as glial cell line-derived neurotrophic factor [50]), or inhibition of factors that prevent rehabilitation (such as chondroitin sulfate proteoglycans [1]), could enhance the differentiation of OM-MSCs into motor neurons at the lesion site. Further studies are needed to investigate whether these combined strategies produce better outcomes than OM-MSCs alone.

In conclusion, OM-MSC administration is an exciting and promising treatment for SCI; however, it requires optimization and standardization.

## DATA AVAILABILITY

Data supporting the findings of this study are available from the corresponding author on reasonable request.

## REFERENCES

1. Francos-Quijorna I, Sanchez-Petidier M, Burnside ER, Badea SR, Torres-Espin A, Marshall L, et al. Chondroitin sulfate proteoglycans prevent immune cell phenotypic conversion and inflammation resolution via TLR4 in rodent models of spinal cord injury. *Nat Commun.* 2022;13:2933.
2. Gao J, Sun Z, Xiao Z, Du Q, Niu X, Wang G, et al. Dexmedetomidine modulates neuroinflammation and improves outcome via alpha2-adrenergic receptor signaling after rat spinal cord injury. *Br J Anaesth.* 2019;123:827–38.
3. Prinz M, Jung S, Priller J. Microglia biology: one century of evolving concepts. *Cell.* 2019;179:292–311.
4. Kwon HS, Koh SH. Neuroinflammation in neurodegenerative disorders: the roles of microglia and astrocytes. *Transl Neurodegener.* 2020;9:42.
5. He T, Li W, Song Y, Li Z, Tang Y, Zhang Z, et al. Sestrin2 regulates microglia polarization through mTOR-mediated autophagic flux to attenuate inflammation during experimental brain ischemia. *J Neuroinflammation.* 2020;17:329.
6. Tan Y, Salkhordeh M, Wang JP, McRae A, Souza-Moreira L, McIntyre L, et al. Thawed mesenchymal stem cell product shows comparable immunomodulatory potency to cultured cells in vitro and in polymicrobial septic animals. *Sci Rep.* 2019;9:18078.
7. Zhuang WZ, Lin YH, Su LJ, Wu MS, Jeng HY, Chang HC, et al. Mesenchymal stem/stromal cell-based therapy: mechanism, systemic safety and biodistribution for precision clinical applications. *J Biomed Sci.* 2021;28:28.
8. Song Y, Wang B, Zhu X, Hu J, Sun J, Xuan J, et al. Human umbilical cord blood-derived MSCs exosome attenuate myocardial injury by inhibiting ferroptosis in acute myocardial infarction mice. *Cell Biol Toxicol.* 2021;37:51–64.
9. He L, He T, Xing J, Zhou Q, Fan L, Liu C, et al. Bone marrow mesenchymal stem cell-derived exosomes protect cartilage damage and relieve knee osteoarthritis pain in a rat model of osteoarthritis. *Stem Cell Res Ther.* 2020;11:276.
10. Assinck P, Duncan GJ, Hilton BJ, Plemel JR, Tetzlaff W. Cell transplantation therapy for spinal cord injury. *Nat Neurosci.* 2017;20:637–47.
11. Takahashi A, Nakajima H, Uchida K, Takeura N, Honjoh K, Watanabe S, et al. Comparison of mesenchymal stromal cells isolated from murine adipose tissue and bone marrow in the treatment of spinal cord injury. *Cell Transplant.* 2018;27:1126–39.
12. Delorme B, Nivet E, Gaillard J, Haupl T, Ringe J, Deveze A, et al. The human nose harbors a niche of olfactory ectomesenchymal stem cells displaying neurogenic and osteogenic properties. *Stem Cells Dev.* 2010;19:853–66.
13. Lindsay SL, Johnstone SA, Mountford JC, Sheikh S, Allan DB, Clark L, et al. Human mesenchymal stem cells isolated from olfactory biopsies but not bone enhance CNS myelination in vitro. *Glia.* 2013;61:368–82.
14. Guo Z, Draheim K, Lyle S. Isolation and culture of adult epithelial stem cells from human skin. *J Vis Exp.* 2011:2561.
15. Nivet E, Vignes M, Girard SD, Pierrisnard C, Baril N, Deveze A, et al. Engraftment of human nasal olfactory stem cells restores neuroplasticity in mice with hippocampal lesions. *J Clin Invest.* 2011;121:2808–20.
16. Huang Y, Tan F, Zhuo Y, Liu J, He J, Duan D et al. Hypoxia-preconditioned olfactory mucosa mesenchymal stem cells abolish cerebral ischemia/reperfusion-induced pyroptosis and apoptotic death of microglial cells by activating HIF-1 $\alpha$ . *Aging.* 2020;12:10931–50.
17. Lindsay SL, Barnett SC. Are nestin-positive mesenchymal stromal cells a better source of cells for CNS repair? *Neurochem Int.* 2017;106:101–7.
18. Lindsay SL, Johnstone SA, McGrath MA, Mallinson D, Barnett SC. Comparative miRNA-based fingerprinting reveals biological differences in human olfactory mucosa- and bone-marrow-derived mesenchymal stromal cells. *Stem Cell Rep.* 2016;6:729–42.
19. Lindsay SL, Toft A, Griffin J, M M Emraja A, Barnett SC, Riddell JS, et al. Human olfactory mesenchymal stromal cell transplants promote remyelination and earlier improvement in gait co-ordination after spinal cord injury. *Glia.* 2017;65:639–56.
20. Ge L, Jiang M, Duan D, Wang Z, Qi L, Teng X, et al. Secretome of olfactory mucosa mesenchymal stem cell, a multiple potential stem cell. *Stem Cells Int.* 2016;2016:1243659.

21. Li M, Rong ZJ, Cao Y, Jiang LY, Zhong D, Li CJ, et al. Utx regulates the NF-kappaB signaling pathway of natural stem cells to modulate macrophage migration during spinal cord injury. *J Neurotrauma*. 2020;38:353–64.
22. Liu Z, Li H, Hong C, Chen M, Yue T, Chen C, et al. ALS-associated E478G mutation in human OPTN (Optineurin) promotes inflammation and induces neuronal cell death. *Front Immunol*. 2018;9:2647.
23. Girard SD, Deveze A, Nivet E, Gepner B, Roman FS, Feron F. Isolating nasal olfactory stem cells from rodents or humans. *J Vis Exp*. 2011;22:2762.
24. Hong CG, Chen ML, Duan R, Wang X, Pang ZL, Ge LT et al. Transplantation of nasal olfactory mucosa mesenchymal stem cells benefits Alzheimer's disease. *Mol Neurobiol*. 2022;59:7323–36.
25. Zhou X, Wahane S, Friedl MS, Kluge M, Friedel CC, Avrampou K, et al. Microglia and macrophages promote corallating, wound compaction and recovery after spinal cord injury via Plexin-B2. *Nat Neurosci*. 2020;23:337–50.
26. Bauman E, Feijao T, Carvalho DTO, Granja PL, Barrias CC. Xeno-free pre-vascularized spheroids for therapeutic applications. *Sci Rep*. 2018;8:230.
27. Lin CS, Xin ZC, Dai J, Lue TF. Commonly used mesenchymal stem cell markers and tracking labels: limitations and challenges. *Histol Histopathol*. 2013;28:1109–16.
28. Karahan G, Kaya H, Eyceyurt RS, Erdogan MA, Yigiturk G, Erbas O. Dexpanthenol reduces fibrosis and aids repair following nerve laceration and neurotaphy. *Exp Ther Med*. 2021;21:207.
29. Liu W, Rong Y, Wang J, Zhou Z, Ge X, Ji C, et al. Exosome-shuttled miR-216a-5p from hypoxic preconditioned mesenchymal stem cells repair traumatic spinal cord injury by shifting microglial M1/M2 polarization. *J Neuroinflammation*. 2020;17:47.
30. Rowald A, Komi S, Demesmaeker R, Baaklini E, Hernandez-Charpak SD, Paoles E, et al. Activity-dependent spinal cord neuromodulation rapidly restores trunk and leg motor functions after complete paralysis. *Nat Med*. 2022;28:260–71.
31. Anderson MA, O'Shea TM, Burda JE, Ao Y, Barlately SL, Bernstein AM, et al. Required growth facilitators propel axon regeneration across complete spinal cord injury. *Nature*. 2018;561:396–400.
32. Hejrati N, Wong R, Khazaei M, Fehlings MG. How can clinical safety and efficacy concerns in stem cell therapy for spinal cord injury be overcome? *Expert Opin Biol Ther*. 2023;23:883–99.
33. Hoang DM, Pham PT, Bach TQ, Ngo ATL, Nguyen QT, Phan TTK, et al. Stem cell-based therapy for human diseases. *Signal Transduct Target Ther*. 2022;7:272.
34. Hoover MY, Ambrosi TH, Steininger HM, Koepke LS, Wang Y, Zhao L, et al. Purification and functional characterization of novel human skeletal stem cell lineages. *Nat Protoc*. 2023;18:2256–82.
35. Cheng HY, Anggella MR, Lin CH, Wei FC. Toward transplantation tolerance with adipose tissue-derived therapeutics. *Front Immunol*. 2023;14:1111813.
36. Nagamura-Inoue T, Nagamura F. Umbilical cord blood and cord tissue banking as somatic stem cell resources to support medical cell modalities. *Inflamm Regen*. 2023;43:59.
37. Bonnet M, Guiraudie-Capraz G, Marqueste T, Garcia S, Jaloux C, Decherchi P et al. Immediate or delayed transplantation of a vein conduit filled with nasal olfactory stem cells improves locomotion and axogenesis in rats after a peroneal nerve loss of substance. *Int J Mol Sci*. 2020;21:2670.
38. Guest J, Herrera LP, Qian T. Rapid recovery of segmental neurological function in a tetraplegic patient following transplantation of fetal olfactory bulb-derived cells. *Spinal Cord*. 2006;44:135–42.
39. Rosenzweig ES, Brock JH, Lu P, Kumamaru H, Salegio EA, Kadoya K, et al. Restorative effects of human neural stem cell grafts on the primate spinal cord. *Nat Med*. 2018;24:484–90.
40. Li M, Rong ZJ, Cao Y, Jiang LY, Zhong D, Li CJ, et al. Utx regulates the NF-kappaB signaling pathway of natural stem cells to modulate macrophage migration during spinal cord injury. *J Neurotrauma*. 2021;38:353–64.
41. Veron AD, Bienboire-Frosini C, Girard SD, Sadelli K, Stamegna JC, Khrestchatsky M, et al. Syngeneic transplantation of olfactory ectomesenchymal stem cells restores learning and memory abilities in a rat model of global cerebral ischemia. *Stem Cells Int*. 2018;2018:2683969.
42. Hamidabadi HG, Simorgh S, Kamrava SK, Namjoo Z, Bagher Z, Bojnordi MN, et al. Promoting motor functions in a spinal cord injury model of rats using transplantation of differentiated human olfactory stem cells: a step towards future therapy. *Behav Brain Res*. 2021;405:113205.
43. Lu D, Xu Y, Liu Q, Zhang Q. Mesenchymal stem cell-macrophage crosstalk and maintenance of inflammatory microenvironment homeostasis. *Front Cell Dev Biol*. 2021;9:681171.
44. Liu Y, Zeng R, Wang Y, Huang W, Hu B, Zhu G, et al. Mesenchymal stem cells enhance microglia M2 polarization and attenuate neuroinflammation through TSG-6. *Brain Res*. 2019;1724:146422.
45. Zhao Y, Gan Y, Xu G, Yin G, Liu D. MSCs-derived exosomes attenuate acute brain injury and inhibit microglial inflammation by reversing CysLT2R-ERK1/2 mediated microglia M1 polarization. *Neurochem Res*. 2020;45:1180–90.
46. Lindsay SL, McCanney GA, Willison AG, Barnett SC. Multi-target approaches to CNS repair: olfactory mucosa-derived cells and heparan sulfates. *Nat Rev Neurol*. 2020;16:229–40.
47. Assunção Silva RC, Pinto L, Salgado AJ. Cell transplantation and secretome based approaches in spinal cord injury regenerative medicine. *Med Res Rev*. 2022;42:850–96.
48. Xun C, Ge L, Tang F, Wang L, Zhuo Y, Long L, et al. Insight into the proteomic profiling of exosomes secreted by human OM-MSCs reveals a new potential therapy. *Biomed Pharmacother*. 2020;131:110584.
49. Gomes ED, Mendes SS, Leite-Almeida H, Gimble JM, Tam RY, Shoichet MS, et al. Combination of a peptide-modified gellan gum hydrogel with cell therapy in a lumbar spinal cord injury animal model. *Biomaterials*. 2016;105:38–51.
50. Cao L, Liu L, Chen ZY, Wang LM, Ye JL, Qiu HY, et al. Olfactory ensheathing cells genetically modified to secrete GDNF to promote spinal cord repair. *Brain*. 2004;127:535–49.
51. Zhang L, Zhuang X, Kotitalo P, Keller T, Krzyczmonik A, Haaparanta-Solin M, et al. Intravenous transplantation of olfactory ensheathing cells reduces neuroinflammation after spinal cord injury via interleukin-1 receptor antagonist. *Theranostics*. 2021;11:1147–61.
52. Jiang Y, Guo J, Tang X, Wang X, Hao D, Yang H. The immunological roles of olfactory ensheathing cells in the treatment of spinal cord injury. *Front Immunol*. 2022;13:881162.
53. Barton MJ, John JS, Clarke M, Wright A, Ekberg J. The Glia response after peripheral nerve injury: a comparison between Schwann cells and olfactory ensheathing cells and their uses for neural regenerative therapies. *Int J Mol Sci*. 2017;18:287.
54. Cofano F, Boido M, Monticelli M, Zenga F, Ducati A, Vercelli A et al. Mesenchymal stem cells for spinal cord injury: current options, limitations, and future of cell therapy. *Int J Mol Sci*. 2019;20:2698.
55. Zachar L, Bačenková D, Rosocha J. Activation, homing, and role of the mesenchymal stem cells in the inflammatory environment. *J Inflamm Res*. 2016;9:231–40.
56. Qu J, Zhang H. Roles of mesenchymal stem cells in spinal cord injury. *Stem Cells Int*. 2017;2017:5251313.
57. Hong HS, Lee J, Lee E, Kwon YS, Lee E, Ahn W, et al. A new role of substance P as an injury-inducible messenger for mobilization of CD29(+) stromal-like cells. *Nat Med*. 2009;15:425–35.
58. Pelagalli A, Nardelli A, Lucarelli E, Zannetti A, Brunetti A. Autocrine signals increase ovine mesenchymal stem cells migration through Aquaporin-1 and CXCR4 overexpression. *J Cell Physiol*. 2018;233:6241–9.
59. Petit I, Szyper-Kravitz M, Nagler A, Lahav M, Peled A, Habler L, et al. G-CSF induces stem cell mobilization by decreasing bone marrow SDF-1 and up-regulating CXCR4. *Nat Immunol*. 2002;3:687–94.
60. Girard SD, Virard I, Lacassagne E, Paumier JM, Lahlou H, Jabes F, et al. From blood to lesioned brain: an in vitro study on migration mechanisms of human nasal olfactory stem cells. *Stem Cells Int*. 2017;2017:1478606.
61. Zhang L, Zhuang X, Chen Y, Xia H. Intravenous transplantation of olfactory bulb ensheathing cells for a spinal cord hemisection injury rat model. *Cell Transplant*. 2019;28:1585–602.
62. Bagher Z, Atoufi Z, Alizadeh R, Farhadi M, Zarrintaj P, Moroni L, et al. Conductive hydrogel based on chitosan-aniline pentamer/gelatin/agarose significantly promoted motor neuron-like cells differentiation of human olfactory ectomesenchymal stem cells. *Mater Sci Eng C Mater Biol Appl*. 2019;101:243–53.

## AUTHOR CONTRIBUTIONS

ZZL and XW conceived the study, designed the experimental procedures, analyzed the data, and prepared the manuscript. XW, CGH, RD, ZLP, and MNZ performed the experiments. HX provided the platform for the experiments, and ZZL and HX supervised the project.

## FUNDING

This work was supported by grants from the National Natural Science Foundation of China (grant numbers 82172502 and 81974127).

## COMPETING INTERESTS

The authors declare no competing interests.

## ETHICS APPROVAL

Animal experiments were approved by the Ethical Review Board of Xiangya Hospital of Central South University (No. 2017121175).

**ADDITIONAL INFORMATION**

**Supplementary information** The online version contains supplementary material available at <https://doi.org/10.1038/s41393-024-01004-6>.

**Correspondence** and requests for materials should be addressed to Hui Xie or Zheng-Zhao Liu.

**Reprints and permission information** is available at <http://www.nature.com/reprints>

**Publisher's note** Springer Nature remains neutral with regard to jurisdictional claims in published maps and institutional affiliations.

Springer Nature or its licensor (e.g. a society or other partner) holds exclusive rights to this article under a publishing agreement with the author(s) or other rightsholder(s); author self-archiving of the accepted manuscript version of this article is solely governed by the terms of such publishing agreement and applicable law.